

Ultrashort Photonic Crystal Optical Switch Actuated by a Microheater

Daryl M. Beggs, Thomas P. White, Lee Cairns, Liam O'Faolain, and Thomas F. Krauss

Abstract—We demonstrate a silicon photonic crystal (PhC) optical switch with a 20- μ s response time controlled by a thermo-optic microheater. The switch consists of a dispersion engineered PhC directional coupler that is only 4.9 μ m long. Optical and electrical isolation is provided by backfilling the holes and embedding the PhC in a silica cladding to produce a vertically symmetric structure that is more robust than a membrane geometry. No increase in optical loss is observed due to the silica cladding, despite operating above the lightline; the insertion loss for airbridge and silica embedded structures are comparable at 1–2 dB.

Index Terms—Directional coupler, integrated optics, optical switching, photonic crystals (PhCs), slow-light.

I. INTRODUCTION

OPTICAL switching is an essential operation for high-speed communication networks. For such applications, efficiency, low power consumption, and robustness are important requirements. In recent years, a number of photonic crystal (PhC)-based devices have been proposed as compact, low power switches [1]–[5], but many of these rely on a membrane geometry that is susceptible to damage and difficult to integrate with other components. Designs based on silica-on-insulator (SOI) PhCs are more robust, but the asymmetric cladding geometry allows coupling between modes that are orthogonal in the membrane structures, and hence increased losses. The lower index contrast between the silica and the silicon also reduces the available bandwidth below the silica lightline, above which losses to radiation modes in the cladding can also be an issue.

Here we demonstrate a compact optical switch based on a Si PhC directional coupler fully embedded in a symmetric silica cladding. This geometry provides protection from the environment and also enables easy integration with additional components such as microheaters or electrical contacts. While the ultimate aim for high-speed operation will be actuation of the switch by free carrier modulation [6]–[8], here thermo-optic tuning is used to demonstrate switching. The design of the switch is compatible with either switching method, and the

Manuscript received July 03, 2008; revised September 02, 2008. First published October 31, 2008. Current version published January 05, 2009. This work was supported by the EU FP6-FET “SPLASH” project. Technical support was provided by the Nanostructuring Platform of EU FP6-NoE “epixnet” (<http://www.nanophotonics.eu>). The work of T. P. White was supported by the EU-FP6 Marie Curie Fellowship “SLIPPRY”.

The authors are with the School of Physics and Astronomy, University of St. Andrews, St. Andrews, KY16 9SS, U.K. (e-mail: daryl.beggs@st-andrews.ac.uk; tom.white@st-andrews.ac.uk; lc273@st-andrews.ac.uk; jww1@st-andrews.ac.uk; tfk@st-andrews.ac.uk).

Color versions of one or more of the figures in this letter are available online at <http://ieeexplore.ieee.org>.

Digital Object Identifier 10.1109/LPT.2008.2008104

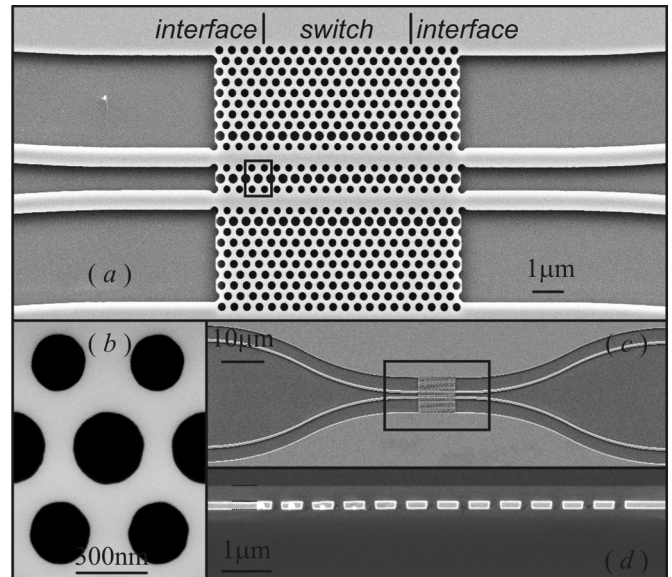


Fig. 1. (a)–(c) Scanning electron micrographs of the PhC directional coupler etched into the silicon, before silica infilling. (a) Shows the design of the switch, which has a length of $12a = 4.9 \mu\text{m}$ (the central region, as marked). At the input/output, interface regions are used to couple light from the slab waveguides into the switching regions. (b) Shows detail of the three hole sizes used for engineering the bandstructure. Most holes are designed with a radius $r_0 = 0.34a$. The smaller holes have $r_1 = 0.31a$, and the larger holes $r_2 = 0.39a$. (c) Shows the on-chip layout: s-bends are used to prevent interaction between the slab waveguides. (d) A cross-section of the PhC after etching and silica infilling.

faster operation using free carriers will require the essential components that are demonstrated in this letter, namely integrated electrical components and a silica-embedded design. The directional coupler design is based on the Si membrane PhC switch reported in [1], where the dispersion of the supermodes of the coupled system were engineered through a control of the hole sizes in the PhC waveguides. In the present work, we demonstrate similar performance in the silica-clad geometry [9], and illustrate the switching behaviour by incorporating an integrated microheater.

II. DESIGN AND FABRICATION

The device presented here is based on that given in [1], [2] (Fig. 1). The lattice constant a is set at 410 nm for 1550-nm wavelength operation. The switching length depends on the splitting of the odd and even modes: $L_{\text{switch}} = \pi/\Delta k$, where Δk is the difference in propagation constants of the two supermodes. The task is to provide a dispersion diagram that maximizes the change in wavevector for a minimum change in frequency or refractive index—this condition is met by the engineered dispersion diagram shown in Fig. 2, calculated using

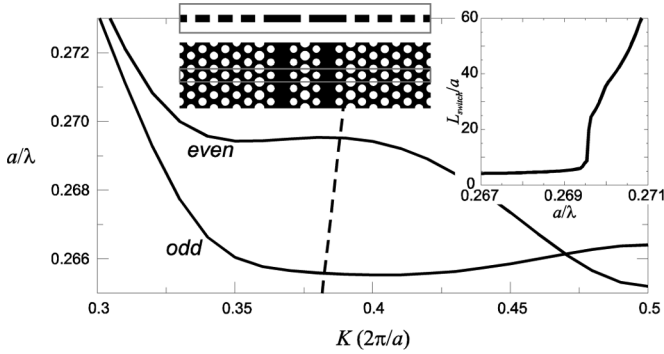


Fig. 2. Dispersion curves of the modes of the central section of the directional coupler switch, calculated using the supercell shown (dimensions $11a\sqrt{3} \times a \times 4h$). The dashed line indicates the position of the lightline of the silica cladding. (Inset) Switching length, directly calculated from the bandstructure using the equation $L_{\text{switch}} = \pi/\Delta k$.

a three-dimensional plane-wave method [10]. Also shown in Fig. 2 (inset) is the switching length, obtained directly from the calculated dispersion curves. At a normalized frequency of $a/\lambda = 0.2695$, it can be seen that the switching length changes very rapidly from over $24a$ (at higher frequencies) to $6a$ (at lower frequencies). Thus, a device with a length between $6a$ and $24a$ will show cross-coupling near the frequency $a/\lambda = 0.2695$ (a wavelength of 1521 nm for $a = 410$ nm). In practice, however, the first cross-coupling peak occurs slightly below this transition frequency, namely at $a/\lambda = 0.267$, due to finite length effects that are not taken into account in the band structure calculation.

The design also includes interface regions consisting of the same PhC geometry stretched along the direction of the waveguide, which allow better coupling of light from the slab waveguides into the PhC switch. By keeping the same hole sizes in the stretched interface heterostructure, the mode profiles between the two PhC regions are better matched, ensuring minimal back reflections from the interface.

The fabrication of the devices proceeds as follows. A 350-nm-thick layer of ZEP-520A is spun onto an SOITEC SOI wafer (220 nm \pm 5-nm-thick Si layer, 2- μ m SiO₂ buffer) to act as a resist and etch mask. The patterns were generated by electron beam lithography, and transferred directly into the Si layer using low-power, low-dc bias reactive ion etching in a CHF₃-SF₆ gas mix, a process known to yield very low-loss PhC waveguides [11]. A silica overlayer and the infilling of the etched structures is provided by a spin-on flowable oxide containing hydrogen silsesquioxane [12], commercially available from Dow Corning as FOx-14. After being hard-baked at 400 °C for 3 h, a planarized layer of low-dielectric material of thickness 500–600 nm is left, as shown in the cross-section of Fig. 1(d).

III. RESULTS AND DISCUSSION

The devices were characterized using an end-fire setup with a broadband light-emitting-diode source. Fig. 3 shows the transmission spectra of both the through (red) and cross (blue) ports of the device, as well as the extinction ratio (top), defined as the ratio of power in the cross-port to that in the through-port. This

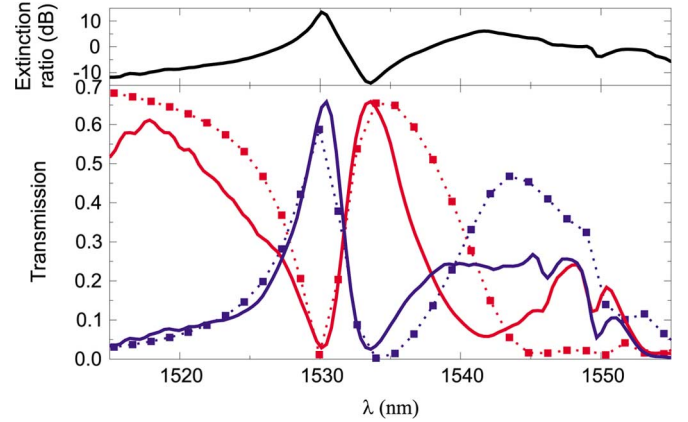


Fig. 3. Measured transmission spectra (bottom) of the through port (red) and the cross port (blue) for the PhC directional coupler after silicon infilling. The transmission axis is normalized to the mean transmission of several 3- μ m-wide slab waveguides. Calculated finite-difference time-domain spectra are also shown (dotted lines and squares). Also shown (top) is the extinction ratio, defined as the ratio of power in the cross-port to that in the through-port.

extinction ratio varies from 14 dB at $\lambda = 1530$ nm to -14 dB at $\lambda = 1533$ nm.

Altering the refractive index of the silicon slab in the local region of the switch shifts the spectrum to longer wavelengths while maintaining its shape [1]. By choosing an operating wavelength of 1533 nm, the output will then switch ports of the device. The refractive index change required to actuate the switch is 6.8×10^{-3} , corresponding to a temperature difference of 38 K.

Fig. 3 also shows spectra calculated using a three-dimensional finite-difference time-domain method. The simulation domain included short lengths of ridge waveguide at either end of the device but did not include the s-bends or the extended access waveguides used in the experimental measurements. The numerical results presented in this letter were calculated for $r_0 = 0.336a$, $r_1 = 0.306a$, and $r_2 = 0.392a$, values obtained after measurements of reference W1 waveguides [13], and a slab height of $h = 220$ nm. The calculations used a grid size of $a/32$ in the plane of the slab and $h/20$ in the out-of-plane direction. The transmission axis is scaled according to the measured insertion efficiency, and there are no free parameters used to fit the results. The excellent agreement between experimental and theoretical spectra attests not only to the high fabrication quality of the devices but also to the accuracy with which the hole sizes are known.

The on-chip insertion efficiency is around 65%, corresponding to an insertion loss of ~ 2 dB. The insertion loss of this device is interesting: as can be seen from Fig. 2, much of the dispersion curves of the relevant modes of the switch lie above the silica lightline, and hence the index confinement in the silicon slab is lost and the modes become “leaky.” This could be expected to significantly increase the insertion loss as compared to an equivalent membrane or air-bridge device. However, it can be seen that the insertion loss reported here is similar to the membrane devices in [1]. We attribute this to the ultrashort length of the switch since losses above the lightline are proportional to the propagation length. Additional measurements on multiple devices would be required to quantify any difference in insertion loss between the two classes of device.

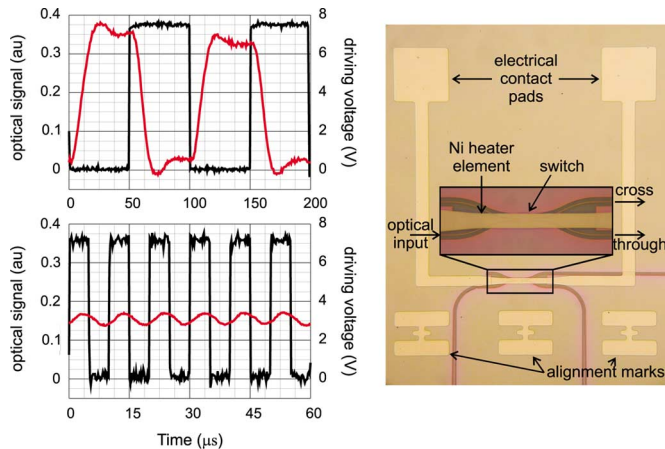


Fig. 4. Left: time response of the through-port of the device (red) when switched on/off at a frequency of 10 kHz (top) and 100 kHz (bottom). The driving signal is also shown (black). Right: a photograph of the microheaters and electrical contact pads.

To demonstrate switching, (nominally) identical devices were fabricated with integrated microheaters consisting of a nickel heating element with a cross-section of $50 \text{ nm} \times 5 \text{ }\mu\text{m}$ as shown by the photograph in Fig. 4. The nickel was deposited directly onto the silica cladding and patterned using a photolithography and lift-off process. A tunable laser set to the operating wavelength was used as input, and switching was achieved by passing a current through the element, locally heating the PhC below. Fig. 4 (left) shows the measured optical response of the output port of the device, as it is driven at 10 kHz (top) and 100 kHz (bottom). The on-state corresponds to passing a current of 21 mA through the heater with an applied potential of 8 V. This is sufficient to shift the transmission spectrum to longer wavelengths such that the transmission into the output ports is reversed. From these measurements, we estimate the response time of the switch to be approximately $20 \text{ }\mu\text{s}$. This is comparable with other thermo-optic devices based on SOI [14]–[16], which have rise times of $5\text{--}60 \text{ }\mu\text{s}$. Although the engineering details of the microheater design remain to be optimized, the response time is likely to be limited by the heat diffusion through the (insulating) layer of silica. Examples of faster (100 ns) and more efficient (2-mW electrical power) switching using the thermo-optic effect have been demonstrated by heating waveguides directly via currents carried by carriers in the doped silicon [3].

IV. CONCLUSION

We have demonstrated an optical switch based on a PhC directional coupler in the silicon-on-insulator material system.

The switch was actuated thermo-optically using an integrated micro-heater. The key insight we gained is that it is possible to realize an all-silica embedded version of the device demonstrated previously [1] with metallic wires in close proximity (500 nm) to the waveguide, without loss of performance. We believe that this demonstration is an essential stepping stone towards the successful demonstration of a PhC switch based on free carrier modulation.

REFERENCES

- [1] D. M. Beggs, T. P. White, L. O'Faolain, and T. F. Krauss, "Ultra-compact and low-power optical switch based on silicon photonic crystals," *Opt. Lett.*, vol. 33, no. 2, pp. 147–149, 2008.
- [2] N. Yamamoto, T. Ogawa, and K. Komori, "Photonic crystal directional coupler switch with small switching length and wide bandwidth," *Opt. Express*, vol. 14, no. 3, pp. 1223–1229, 2006.
- [3] Y. A. Vlasov, M. O'Boyle, H. F. Hamann, and S. J. McNab, "Active control of slow light on a chip with photonic crystal waveguides," *Nature*, vol. 438, pp. 65–69, 2005.
- [4] M. Tinker and J.-B. Lee, "Thermal and optical simulation of a photonic crystal light modulator based on the thermo-optic shift of the cut-off frequency," *Opt. Express*, vol. 13, no. 18, pp. 7174–7188, 2005.
- [5] E. A. Camargo, H. M. H. Chong, and R. M. De La Rue, "Highly compact asymmetric Mach-Zehnder device based on channel guides in a two-dimensional photonic crystal," *Appl. Opt.*, vol. 45, no. 25, pp. 6507–6510, 2006.
- [6] W. M. J. Green, M. J. Rooks, L. Sekaric, and Y. A. Vlasov, "Ultra-compact, low RF power, 10 Gb/s silicon Mach-Zehnder modulator," *Opt. Express*, vol. 15, no. 25, pp. 17106–17113, 2007.
- [7] A. Liu, L. Liao, D. Rubin, H. Nguyen, B. Ciftcioglu, Y. Chetrit, N. Izhaky, and M. Paniccia, "High-speed optical modulation based on carrier depletion in a silicon waveguide," *Opt. Express*, vol. 15, no. 2, pp. 660–668, 2007.
- [8] L. Gu, W. Jiang, X. Chen, L. Wang, and R. T. Chen, "High speed silicon photonic crystal waveguide modulator for low voltage operation," *Appl. Phys. Lett.*, vol. 90, p. 071105, 2007.
- [9] T. P. White, L. O'Faolain, J. Li, L. C. Andreani, and T. F. Krauss, "Silica-embedded silicon photonic crystal waveguides," *Opt. Express*, vol. 16, pp. 17076–17081, 2008.
- [10] S. G. Johnson and J. D. Joannopoulos, "Block-iterative frequency domain methods for Maxwell's equations in a planewave basis," *Opt. Express*, vol. 8, no. 3, pp. 173–190, 2000.
- [11] L. O'Faolain, X. Yuan, D. McIntyre, S. Thoms, H. Chong, R. M. De la Rue, and T. F. Krauss, "Low-loss propagation in photonic crystal waveguides," *Electron. Lett.*, vol. 42, no. 25, pp. 1454–1455, 2006.
- [12] C.-C. Yang and W.-C. Chen, "The structures and properties of hydrogen silsesquioxane (HSQ) films produced by thermal curing," *J. Mater. Chem.*, vol. 12, pp. 1138–1141, 2002.
- [13] D. M. Beggs, L. O'Faolain, and T. F. Krauss, "Accurate determination of the functional hole size in photonic crystal slabs using optical methods," *Photonics and Nanostructures—Fundamentals and Applications*, vol. 6, no. 3–4, pp. 213–218, 2008.
- [14] U. Fischer, T. Zinke, B. Schuppert, and K. Petermann, "Singlemode optical switches based on SOI waveguides with large cross-section," *Electron. Lett.*, vol. 30, no. 5, pp. 406–408, 1994.
- [15] G. V. Treyz, "Silicon Mach-Zehnder waveguide interferometers operating at $1.3 \text{ }\mu\text{m}$," *Electron. Lett.*, vol. 27, no. 2, pp. 118–120, 1991.
- [16] J. Xia, J. Yu, Z. Wang, Z. Fan, and S. Chen, "Low power 2×2 thermo-optic SOI waveguide switch fabricated by anisotropy chemical etching," *Opt. Commun.*, vol. 232, pp. 223–228, 2004.